Separating the ferromagnetic and glassy behavior within the metal-organic magnet Ni(TCNQ)₂

Adam Berlie,[1,2,3,*] Ian Terry,[3] Marek Szablewski,[3] and Sean R. Giblin[4]

[1]*ISIS Neutron and Muon Facility, Science and Technology Facility Council, Chilton, Oxfordshire, OX11 0QX, United Kingdom*

[2]*Advanced Meson Science Laboratory, RIKEN Nishina Center for Accelerator-Based Science, 2-1 Hirosawa, Wako, Saitama 351-0198, Japan*

[3]*Department of Physics, Durham University, South Road, Durham, DH1 3LE, United Kingdom*

[4]*School of Physics and Astronomy, Cardiff University, Queens Buildings, The Parade, Cardiff, CF24 3AA, United Kingdom*

An in-depth study of the metal-organic magnet Ni(TCNQ)₂ was conducted where the deuterated form was synthesised both to attempt to alter the magnetic properties of the material and to be advantageous in techniques such as neutron scattering and muon spectroscopy. Deuteration saw a 3 K increase in T_C with magnetization and heat capacity measurements demonstrating a spin wave contribution at low temperatures confirming the 3D nature of the ferromagnetic state shown by $Ni(TCNQ - D_4)_2$. AC susceptibility results suggest there is a glassy component associated with the magnetically ordered state, though muon spectroscopy measurements did not support the presence of a spin glass state. Instead muon spectroscopy at zero magnetic field indicated the presence of two magnetic transitions, one at 20 K and another below 6 K; the latter is likely due to the system entering a quasistatic regime, similar to what one might expect of a superspin or cluster glass. Neutron diffraction measurements further supported this by revealing very weak magnetic Bragg peaks suggesting that the magnetism may have a short coherence length and be confined to small grains or clusters. The separation of the ferromagnetic and glassy magnetic components of the material's properties suggest that this system may show promise as a metal-organic magnet which is easily modified to change its magnetic properties, providing larger grain sizes can be synthesized.

PACS number(s): 75.10.Nr, 75.50.Lk, 75.50.Xx, 76.75.+i

I. INTRODUCTION

Organic based magnetism presents great advantages over conventional inorganic materials due to the tunability of the organic component. For example, charge transfer systems have been used to create exotic magnets with the organic component acting as an exchange pathway between metal ions [1,2]. [Fe(Cp*)₂][TCNE] (Cp* = C₅Me₅, pentamethyl-cyclopentadienide, TCNE = tetracyanoethylene) was one of the first charge transfer magnetic compounds to be synthesized where a T_C of 2.55 K was observed [3,4]. When substituting TCNQ (7,7,8,8-tetracyanoquinomethane) [5] for TCNE, the sample shows a complex paramagnetic and metamagnetic phase [6–8], and recrystallizing the sample in acetonitrile at $-20\,°C$ resulted in a bulk 3D ferromagnet where $T_C = 3.1$ K [9]. The chemistry of these systems is incredibly rich where there can be strong solvent dependencies of Fe-Fe intrachain distances, which effects the magnetism [10,11]. The unsolvated product shows large disorder where the AC susceptibility shows a weak frequency dependence, characterized by the parameter φ [12] that ranges from 0.005–0.0085, and so the samples are believed to be weak spin glass materials [11].

One big advancement in metal-organic magnetism was reached with the synthesis of the $M(TCNQ)_2$ series, where M = Fe, Mn, Co, and Ni [13]. The hydrated or solvated product, $M(TCNQ)_2(S)_x$ (where S = solvent), can be easily synthesized and shows paramagnetic behavior [14–16]. However the new unsolvated $M(TCNQ)_2$ samples show clear evidence of crystallinity where the unit cell was indexed to be tetragonal, and, in the case of the Ni compound, the lattice parameters $a = 17.029(5)$ Å and $c = 8.0508(2)$ Å which were obtained from x-ray diffraction data. For the Ni(TCNQ)₂ compound this showed a bulk ferromagnetic transition with a $T_C = 20.8$ K ($\theta = 37$ K), though it is believed that there is a glassy component associated with the magnetic transition. The magnetic glassiness was suggested by both AC susceptibility data as well as a nonzero specific heat capacity as $T \to 0$ which points to residual entropy associated with the magnetism indicative of glassiness [12]. Spin glass behavior in these types of compounds is not uncommon, an example being the quasi-1D material, [MnTPP]⁺[TCNE]⁻$x(1,3 - C_6H_4Cl_2)$ (TTP = tetraphenylprohphyrin) [17,18]. The low temperature glassy phase of this compound was studied further and is believed to be due to magnetic clusters forming outside of the 1D limits within the structure where the frequency dependence of the AC susceptibility was similar to that of the canonical spin glasses [19–21]. Note that Mn(TCNQ)₂ has previously been reported [22,23] where the TCNQ molecules in the unhydrated sample were believed to pair up and go from a triplet to an antiferromagnetically coupled singlet state where, at low temperatures, the reported magnetic moment is close to 5.92 μ_B which is the theoretical prediction if the magnetism is a result of the d electrons located on the Mn (II) ion only; this is different from the result reported by Clérac *et al.* [13].

Vickers *et al.* used a similar method where they produced amorphous $M(TCNQ)_\gamma$ salts [24], and their Ni compound showed an elevated T_C of 31 K. The only difference between the two synthetic procedures was that instead of using a $[BF_4]^{2-}$ counter ion, Vickers *et al.* used a weaker binding anion of $[SbF_6]^{2-}$. The exchange mechanism was thought to be similar to that in V(TCNE)$_x$ yCH₂Cl₂ ($T_C > 350$ K), where the vanadium and TCNE ions are believed to couple antiferromagnetically resulting in the overall ferrimagnetism observed [25]. This ferrimagnetism was shown, in V(TCNE)$_x$,

*adam.berlie@stfc.ac.uk

to be 3D in nature in both thin film and bulk form [26], however there is evidence for structural disorder from included diamagnetic solvent molecules within the structure [27,28], where similar systems showed changes in the magnetism when the electron acceptor was manipulated [29]. Nevertheless this exchange mechanism may show strong parallels to the $M(TCNQ)_2$ systems. At low temperatures the system showed characteristics of a correlated spin glass [26] where, in the bulk system, this was attributed to random atomic clusters.

Within this paper we report a detailed study of $Ni(TCNQ)_2$ to attempt to obtain further information on the magnetic state of this charge transfer salt, particularly the apparent spin glass component reported in earlier studies. Both the protio and deuterated product were synthesized, with more attention being paid to the new deuterated material, which can be regarded as a simple molecular change to see if subtle changes to the TCNQ aromatic ring can alter the magnetism. Magnetic susceptibility measurements were conducted using both an DC and AC technique where, on deuteration, there was an observed shift in T_C by $+3$ K. AC susceptibility revealed that on two different samples there are different frequency dependencies in the real component which suggests different degrees of disorder within each system. To further study the material muon spin relaxation (μSR) was used where two magnetic transitions were observed, one that corresponds to a ferromagnetic transitions at $\sim$20 K and another at lower temperatures of $\sim$6 K, where the system enters a quasistatic regime, and it is proposed that there are interactions between ferromagnetic regions that freeze out, thus leading to a cluster glass type material.

II. EXPERIMENTAL

$Ni(TCNQ)_2$ was synthesized under an inert argon atmosphere following a similar method to that previously reported by Clérac *et al.* [13]. $TCNQ - D_4$ was prepared using a method described by Dolphin *et al.* [30], where the products made were confirmed using NMR and UV-vis spectroscopy.

DC magnetic measurements were taken on a Quantum Design MPMS 5XL with a temperature range of 2–360 K and an applied field range of -5 to 5 T. AC magnetic susceptibility and heat capacity studies were conducted on a Quantum Design PPMS. For the AC susceptibility experiment the frequency of the field was varied (between 10 and 10000 Hz) with a fixed amplitude of 10 μT. The PPMS was also used to measure the heat capacity of $Ni(TCNQ - D_4)_2$ using the isothermal relaxation method.

Structural investigations on the deuterated sample were conducted using both x-ray and neutron sources. Powder x-ray diffraction (PXRD) was carried out using the I11 high resolution powder diffraction beam line at the Diamond Light Source. D1B at the Institute Laue-Langevin, a high flux neutron diffractometer, was used to study the possibility of any long range magnetic ordering associated with the crystal structure. Muon spin relaxation (μSR) experiments were also carried out on the EMU spectrometer at the ISIS neutron and muon source where the sample was mounted on a silver backing plate. A He flow cryostat was used to access low temperatures in both neutron scattering and μSR experiments.

III. RESULTS

The following section will detail the results from various techniques used to study the protio and deuterated compounds. The main focus was on the deuterated sample as this was used in both the neutron and muon experiments.

A. Structural measurements

The x-ray data were used to index the diffraction patterns (shown in the Supplemental Material [31]) where the TREOR90 program from the FULLPROF Suite was used [32,33]. TREOR90 is a trial and error program for indexing powder diffraction patterns which outputs the unit cell parameters and a suggested space group. The only structural information that was possible to gain from the data was that the unit cell is tetragonal where $a = b = 18.11$ Å and $c = 8.51$ Å, which is similar to the results by Clérac *et al.* [13]. The space group was also indexed as $P4/mmm$, though this does not rule out the possibility of an orthorhombic structure with only a very small difference between the a and b lattice parameters since the diffraction peaks were too broad to distinguish between the two structures.

An in-house Siemans D5 diffractometer with a Cu source was used to obtain a diffraction pattern (not shown here) from which the mean particle size was determined using the Scherrer equation [34] to analyze the reflection peak widths. Data in the d-spacing range of 4 to 5 Å suggest a particle size of 31(2) nm.

A neutron diffraction experiment was also attempted to gain information on the magnetic structure of the metal-organic compound, where the D1B diffractometer was used. However, even though a high neutron flux was obtained from the instrument, long counting times of approximately 24 hours per temperature were required to obtain satisfactory counting statistics. Two temperatures were chosen above and below the magnetic transition: 60 K and 1.5 K (cryostat base temperature).

It was not possible to get any detailed structural information from the data, given the low angular resolution and the broad diffraction peaks. However, there was evidence for very weak magnetic peaks at approximately $2\theta = 16°$ and $23°$ as shown in the difference plot of Fig. 1. These weak peaks do not have the typical shape that corresponds to thermal expansion/contraction of the sample (see $2\theta = 43°$), and so it may be possible that we are observing magnetism that has a very short coherence length [35]. The d spacing that the magnetic peaks correspond to are 9.0 and 6.3 Å, respectively, and all these peaks are observed in the XRD data indicating that the corresponding moment may be associated with a Ni^{2+} ion. Using the lattice parameters for the tetragonal unit cell, it is possible to identify the 9.0 Å reflection as corresponding to the planes (200) or (020), etc. The 6.3 Å peak may correspond to either of two sets of planes, (220) or (201); these reflections are very close together, and we cannot distinguish between the two due to the observed broad peaks. However, given that the high d-spacing peak is from the (200) planes, it might be plausible that the lower d-spacing peak is from the (220) plane as this would allow for a similar orientation of the magnetic moment, i.e., along the c axis.
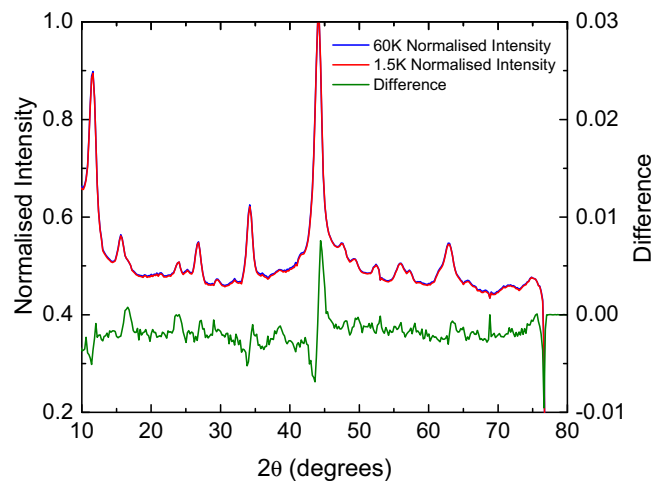
FIG. 1. (Color online) Normalized neutron diffraction data for $Ni(TCNQ-D_4)_2$, where weak magnetic peaks were seen in the difference plot at approximately $2\theta = 16°$ and $23°$.

Recently, scanning tunneling microscopy (STM) was conducted on $Ni-TCNQ_x$ 2D structures [36] synthesized on an Ag(100) substrate. It was found that the Ni atoms and TCNQ molecules coordinate via the cyano groups and, for the 2D structures of the $Ni(TCNQ)_2$ stoichiometry, the Ni atoms were found to sit on the corners of a square 2D face-centered unit cell. The unit cell had a lattice parameter equal to 18.5 Å that is similar to the results obtained by us from our diffraction experiments. Interestingly, the positions of the Ni ions are located within the 2D unit cell (20) and (22) planes, analogous to the planes attributed to magnetic scattering in the bulk $Ni(TCNQ)_2$ sample as noted above.

Scanning electron microscopy (SEM) images (shown in the Supplemental Material [31]) were also taken of both the protio and deuterated sample where there was a remarkable difference in particle size between the two samples. There were slight differences in the chemical reaction during the last step where the deutero product required heating to pass the intermediate intermediate, and reach the product. The fact that this was not required with the protio sample indicates that the energetics of the reaction differ between the two samples. The images for both samples show there is a range of particle sizes, and both samples are made of tiny crystallites. However, on average, the crystallites within the deuterated sample are larger. As deuterating the TCNQ appeared to have a dramatic effect on the reaction kinetics, it may have also caused slower growth of the crystals which would lead to larger particle sizes. The protio sample precipitated out of solution almost immediately upon mixing the reagents which is conducive to producing small particles.

Interestingly, the data from the SEM and diffraction experiments, mentioned above, show contrasting conclusions. This may be explained if there are nanograins, of size 31(2) nm (deduced from PXRD data), which agglomerate to produce the larger structural features that are observable within the SEM images. It is also possible that the structural features are crystallites but with a high degree of disorder leading to only small regions of coherent crystallinity that are taken to be nanograins.

B. Characterization

To study any difference in magnetic properties between the protio and deuterated product, magnetic measurements were performed on the samples. This included both DC and AC susceptibility as well as heat capacity measurements to study the transition region. It is worth noting that all samples were fresh when measured as the sample is known to age when a decrease in T_C is observed due to the absorption of water within the sample [37].

1. Magnetic measurements

The data from the protio and deutero samples are shown in Fig. 2. The most significant change is an increase in T_C of approximately 3 K when the protons are swapped for deuterons. The respective critical temperatures are 17 and 20 K for the protio and deutero product, the Curie temperatures being determined by differentiating the curve within the critical region, fitting a Gaussian peak to the resulting curve and taking the center of the peak to determine accurately the T_C (which is essentially defined as the steepest part of the slope in an M vs T plot). It should be noted that another way to define T_C is from the initial upturn in the magnetization data, which would place it at 28 K for the deutero and 25 K for the protio compounds.

Another striking difference is the low temperature area of the ZFC curves where, at the lowest temperatures, the difference between the ZFC and FC curves is much greater for the protio sample. This may be due to the glassy component of the magnetism which was pointed out by Clérac *et al.* in their original paper [13]. In such a case the magnetic ground state would not be considered to be well defined, and, due to competing interactions, different possible configurations of the magnetic state may be obtainable when the sample is cooled. However, the data support the conclusion that both samples
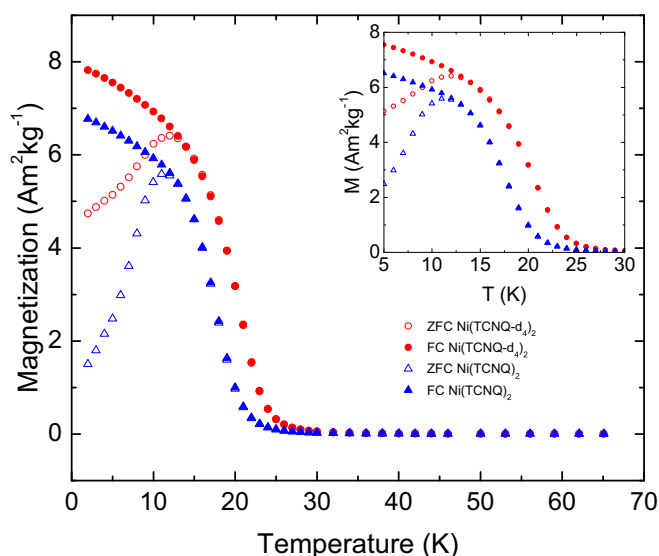
FIG. 2. (Color online) Magnetization vs temperature for both $Ni(TCNQ-H_4)_2$ and $Ni(TCNQ-D_4)_2$ in a field of 2.5 mT (ZFC = zero-field cooled and FC = field cooled). Inset: Expanded view of the magnetically ordered region.
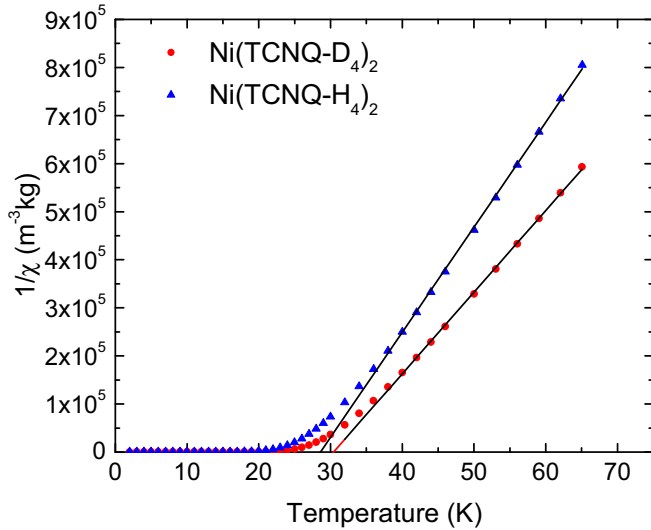
FIG. 3. (Color online) Inverse magnetic susceptibility (field cooled where $B = 2.5$ mT) vs temperature for both the protio and deutero samples of $Ni(TCNQ)_2$. Note that, in both cases, the susceptibility is the measured magnetic susceptibility with the relevant background contribution removed. Solid lines are Curie-Weiss fits to the high temperature data.

are indeed ferromagnetic or ferrimagnetic where, at 2.5 mT, hysteretic behavior is observed. The temperature where the hysteresis is introduced in the system (T_{Div}) also scales with the change in T_C between the protio and deutero samples, where the divergence of the ZFC/FC curves occurs at 11 and 13 K, respectively.

Figure 3 shows the inverse magnetic susceptibility which at high temperatures follows Curie-Weiss behavior where, from Table I, $\theta = 30.4$ K and 28.6 K for the deutero and protio samples, respectively. The positive values of the Curie-Weiss temperatures lend support to the idea that the materials are ferromagnetic in nature. The change in slope suggests that either or both the effective moment and/or the number of magnetic formula units per unit mass has changed. Swapping hydrogen for deuterium will cause the formula unit per mass, or number density (N), to change as deuterium is twice as heavy as hydrogen. If one assumes a molecular formula unit of $Ni(TCNQ)_2$, the effective moments determined from the Curie constants are 4.22 and 3.68 μ_B for the deutero and protio samples, respectively. The difference in these values may be related to the nonstoichiometry of the systems as, from the previous section, the deuterated sample appears more ordered in that

TABLE I. Parameters for $Ni(TCNQ)_2$ from the magnetic data collated for reference, where C = Curie Constant. Errors are given in brackets.

Parameter	$Ni(TCNQ-H_4)_2$	$Ni(TCNQ-D_4)_2$
T_C (K)	17.42(7)	20.17(9)
θ (K)	28.6(1)	30.4(2)
C (m^3 Kkg^{-1})	$4.57(3) \times 10^{-5}$	$5.89(4) \times 10^{-5}$
μ_{eff} (μ_B)	3.68(3)	4.22(4)
T_{Div} (K)	11	13

larger crystallites are observed within the SEM measurement, and so if the sample shows more disorder, this may lower the effective moment. At temperatures above 70 K the inverse susceptibility no longer follows simple linear variation with T. If one follows the same argument for $Ni(TCNQ)_2$ as made for $V(TCNE)_x$, it might be expected that this nonlinearity is a result of a ferrimagnetic interaction between the Ni and TCNQ magnetic moments; the Supplemental Material [31] contains a fit of inverse susceptibility temperature dependence for a simple model describing such a ferrimagnetic response [38].

When calculating the effective moment of $Ni(TCNQ)_2$ one must consider a Ni^{2+} cation and $TCNQ^-$ anion. The spin only formula, assuming quenching of the orbital angular momentum, would then be

$$p_{eff}^2 = g_{Ni^{2+}}^2 \mu_B^2 S_{Ni^{2+}}(S_{Ni^{2+}} + 1)$$
$$+ 2\left[g_{TCNQ^-}^2 \mu_B^2 S_{TCNQ^-}(S_{TCNQ^-} + 1)\right], \quad (1)$$

and assuming $g = 2$ and $S = 1$ for the Ni^{2+} ion and $S = \frac{1}{2}$ for $TCNQ^-$, this results in $p_{eff} = 3.74$ μ_B. Alternatively, in the absence of the quenching of the orbital angular momentum of the Ni^{2+} ion, a ground state moment per formula unit of $p_{eff} = 6.01$ μ_B is obtained. The p_{eff} values shown in Table I are closest to orbital angular momentum-quenched value, with the value of the deuterated sample possibly indicating that a partial quenching of the orbital angular momentum exists in the material.

From mean field theory [39] and using the θ parameter calculated from Curie-Weiss law, one can estimate the exchange constant or coupling strength of the magnetic ions with spins S_1 and S_2, J_{ex}/k_B,

$$\frac{J_{ex}}{k_B} = \frac{3\theta}{2z\sqrt{S_1(S_1 + 1)S_2(S_2 + 1)}}, \quad (2)$$

where z is the nearest neighbor occupancy. Since $\theta = 30.4$ K for the deuterated sample (see Table I) and if $z = 6$ (for an octahedral system) and say $S_1 = 1$ and $S_2 = \frac{1}{2}$, $J_{ex}/k_B = 6.2$ K and if $z = 4$ (for a tetrahedral or square planar system), then $J_{ex}/k_B = 9.3$ K. These parameters will be discussed later in the paper. Note we assume that the exchange coupling is isotropic to obtain an estimate of the magnitude of the exchange constant, and the fine powder nature of the sample prevents us from investigating any anisotropy in the exchange constant.

ZFC magnetic susceptibility of a deuterated sample was measured in an applied field of 0.1 T (see Supplemental Material [31]) aimed to suppress the hysteretic behavior of the material whilst maintaining a well defined ferromagnetic transition. From a Curie-Weiss fit to these data, $\theta = 30.6(1)$ K and $C = 3.97(3) \times 10^{-5}$ m^3 Kkg^{-1}, giving a moment of 3.46(1) μ_B which shows the similarity to the low field magnetization data. The region of interest within this data is at low temperatures (see Fig. 4), as when the data are plotted as a function of $T^{\frac{3}{2}}$ it can be described using Bloch's law,

$$M = M_s(0) - M_s(0)D\left(\frac{T}{T_C}\right)^{\frac{3}{2}}. \quad (3)$$

Here $M_s(0)$ is the spontaneous magnetization at $T = 0$ K in an applied field of 0.1 T (in this case), and D is a constant.
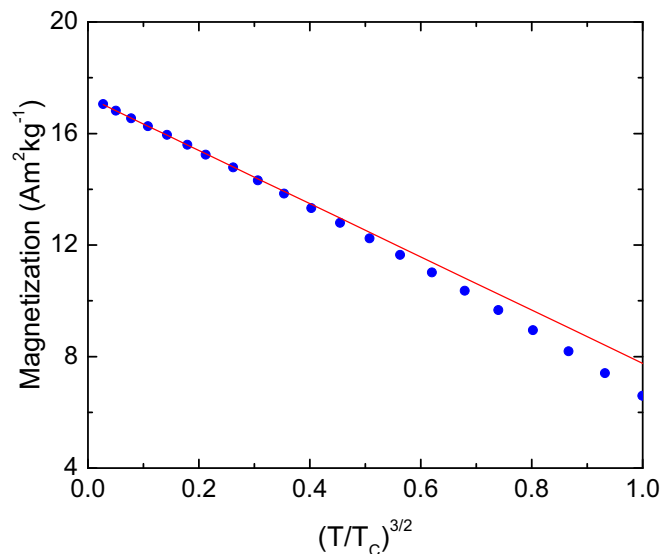
FIG. 4. (Color online) Low temperature data for Ni(TCNQ − D$_4$)$_2$, which can be fitted to Bloch's law [Eq. (3)]. Data were taken with an applied field of 100 mT.

The magnetization is seen to have a $T^{\frac{3}{2}}$ dependence which decreases as T increases due to excitations of 3D spin waves within the material. For the ZFC 0.1 T curve it is possible to fit the above equation to the data at very low temperatures up to about 10 K at which the curves begin to diverge as shown in Fig. 4.

From the fit to the data $M_s(0) = 17.3$ Am^2 kg^{-1} and $D = 0.48$. The fact that the data can be fitted using this straight line equation, although well below T_C, is evidence that the material is falling into a 3D ordered magnetic system at low temperatures. The observation of Bloch's law has been seen in other nanograined and nanoparticulate ferromagnetic and ferrimagnetic materials. However, it is often found that the coefficient of the $T^{\frac{3}{2}}$ term exceeds that of the bulk value which has been attributed to surface and finite size effects [40]. Also, Peng *et al.* [41] have demonstrated the importance of nanograin connectivity in the excitations of long wavelength spin waves (and hence the observation of Bloch's law) in Fe$_x$Ag$_{1-x}$. For a 3D simple cubic ferromagnet consisting of spins of S_1 and S_2, following Bloch's law one can calculate J_{ex}/k_B using the equation [42]

$$\frac{J_{ex}}{k_B} = \left(\frac{0.117 M_s(0)}{(S_1 + S_2)\Delta M} \right)^{\frac{2}{3}} \frac{(S_1 + S_2)T}{4S_1 S_2}, \qquad (4)$$

where $\Delta M = M_s(0) - M$. Using Eq. (3) along with the experimental values $D = 0.48$ and $T_C = 20.17$ K and taking $S_1 = 1$ and $S_2 = \frac{1}{2}$, we obtain $J_{ex}/k_B = 4.5$ K; this value is similar to that calculated from the θ parameter from the Curie-Weiss fit. It should be noted that the value of J_{ex}/k_B determined from Bloch's law assumes that the applied magnetic field is zero. Including a finite magnetic field of 0.1 T results in an exchange constant that is smaller by a factor of about 0.86.

Magnetization data were also taken as a function of applied field to study the field dependent behavior above and below the transition (see Fig. 5). It is clear that as the sample is taken
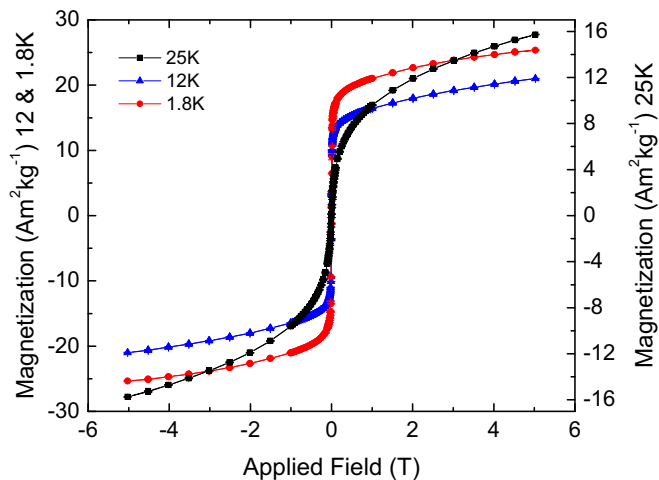
FIG. 5. (Color online) Magnetization vs applied field for the Ni(TCNQ − D4)$_2$ compound. Data were taken at 1.8, 12, and 25 K.

below the transition temperature the response to an applied magnetic field is radically different. The sharp increase in the magnetization as a small field is applied below T_C is consistent with the behavior of a ferromagnetic or ferrimagnetic material indicating the presence of a spontaneous magnetic moment. See Table II for a summary of parameters at the lowest temperature accessible, 1.8 K. Moreover, the approximately linear trend of the magnetization at high fields above the spontaneous magnetization, for $T < T_C$, is indicative of a ferrimagnetic response [2]. At low temperatures the sample shows a spontaneous magnetic moment per formula unit of 1.8 μ_B. For comparison, if one considers a TCNQ anion, the saturation moment for $S = \frac{1}{2}$ would be 1 μ_B, for the Ni^{2+} ion in an $S = 1$ state would have a saturation moment of 2 μ_B while in the absence of a quenched orbital angular momentum this value would be 5 μ_B. Ferromagnetic collinear combinations of these values would yield saturation moments of formula unit to be 4 μ_B and 7 μ_B for the quenched and unquenched orbital moments of Ni^{2+}, respectively. Antiferromagnetic collinear combinations of the moments would yield saturation moments of formula unit to be 0 μ_B and 3 μ_B for the quenched and unquenched orbital moments of Ni^{2+}, respectively.

In all but one case, the expected values of the formula unit saturation moment exceed the value that is observed. The exception predicts a completely compensated combination of

TABLE II. Parameters for Ni(TCNQ)$_2$ from the magnetization as a function of applied field at 1.8 K collated for reference. The subscript Spont = spontaneous magnetization and 5T = the values at a field value of 5 T. Errors are given in brackets.

Parameter	Value
M_{Spont} (Am^{2}kg^{-1})	21.4(1)
M_{5T} (Am^{2}kg^{-1})	25.35(7)
μ_{Spont} (μ_B)	1.8
μ_{5T} (μ_B)	2.1
H_C (mT)	1

magnetic moments, which is not observed in the experiment. However, if the ordering of the magnetic moments was not collinear the spin-only Ni^{2+} moment ferrimagnetically coupled with the TCNQ moments would be expected to result in a nonzero moment per formula unit, especially if there was only a partial orbital quenching of the magnetic moment of the nickel as suggested by the data for $T > T_C$.

The sample shows hysteretic behavior at all three temperatures (see Fig. 5 in the Supplemental Material [31]), where the difference in magnetization depending on the direction of the ramped field is not accounted for by the error in the measurement. Again, one can clearly see the differences in behavior with an applied field between all three temperatures. The hysteretic behavior present at 12 K is typical of a ferromagnetic or ferrimagnetic material, however more data points are needed at low fields in order to study the coercivity; an estimate is $H_C \sim 1$ mT. At the lowest temperature, 1.8 K, the magnetization is different in the first quadrant of the measurement, and the overall curve is asymmetric where perhaps there is a time dependence associated with the sweeping of the magnetic field.

In order to further investigate such time dependencies, AC susceptibility measurements were made to probe the material's magnetic state as a function of applied field frequency and temperature. The AC field was held constant at 10 μT and no external DC field was applied. The frequency of the AC field was varied to probe both the real (χ') and imaginary (χ'') components of the susceptibility. For this study, two different samples (1 and 2) were measured to see whether the dynamic magnetic behavior was consistent between samples. One of the advantages of AC susceptibility experiments is that one can probe the response of the sample at very small applied fields. This is advantageous when investigating, for example, spin glasses [12]. Sample 1 will be discussed first.

In an earlier work, Clérac *et al.* [13] reported that $Ni(TCNQ)_2$ exhibited a glassy magnetic component. This may be quantitatively assessed in $Ni(TCNQ-D_4)_2$ using the "Mydosh" criterion for a spin glass,

$$T_f(\omega) = T_{f0}\varphi \log(\omega) + T_{f0}. \qquad (5)$$

Here T_f denotes the freezing temperature of the spin glass which is attributed to the cusp in the χ' vs T data (see Fig. 6) for a given angular frequency ω of the magnetic field, while between T_C and about 15 K there is no discernible dependence of χ' on the frequency. A plot of T_f vs $\log(\omega)$ yields a straight line where $T_{f0} = 11.52 \pm 0.04$ K and $\varphi = 0.0315 \pm 4 \times 10^{-4}$. The value of φ is about an order of magnitude smaller than that describing the dynamics of noninteracting superparamagnetic particles, though it is consistent with values obtained from spin glasses [12]. However, it is also possible that the value for φ obtained for $Ni(TCNQ-D_4)_2$ may be a consequence of interactions between superparamagnetic particles [43].

A further test for superparamagnetic behavior is to use the Arrhenius law which generally governs a thermally activated process where a fit to the data provides parameters of $\omega_0/2\pi = 1.25 \times 10^{38}$ Hz and $E_a/k_B = 1018$ K; these are clearly unphysical values for a thermally activated process occurring at around 10 to 20 K. This result again suggests that the sample does not behave like a noninteracting superparamagnet.
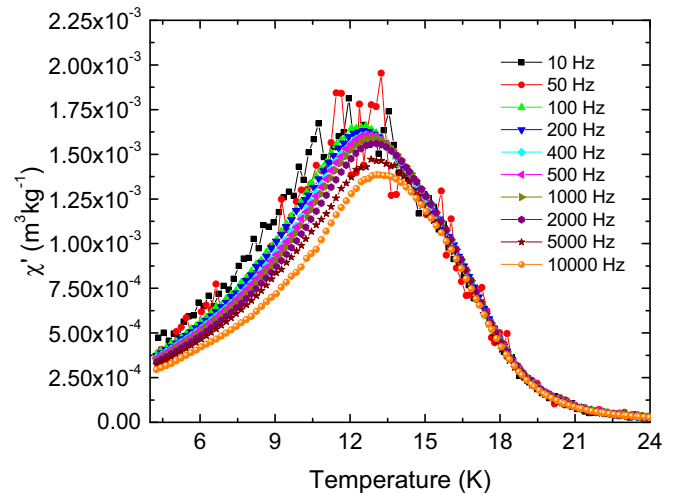
FIG. 6. (Color online) χ' vs temperature for a sample of $Ni(TCNQ-D_4)_2$ showing the frequency dependence of the transition measured with a magnetic field of 10 μT.

An alternative approach is to analyze the data using the Vogel-Fulcher method which is commonly used to describe the dynamics of real glasses and has been used to parametrize the frequency-temperature responses of nonmetallic spin glasses [44] and superspin glasses [45]. Here the dynamics of the system are described by Eq. (6) where T_0 is a fitting parameter. For demonstration purposes, T_0 is set at T_{f0}, taken from the above analysis using the Mydosh parameter φ. The resulting plot, shown in Fig. 7, demonstrated linearity over the midrange of frequencies, and so data points with 10, 5000, and 10000 Hz were not included in the fit to Eq. (6).

$$\omega = \omega_0 \exp\left(\frac{-E_a}{k_B(T_f - T_0)}\right) \qquad (6)$$
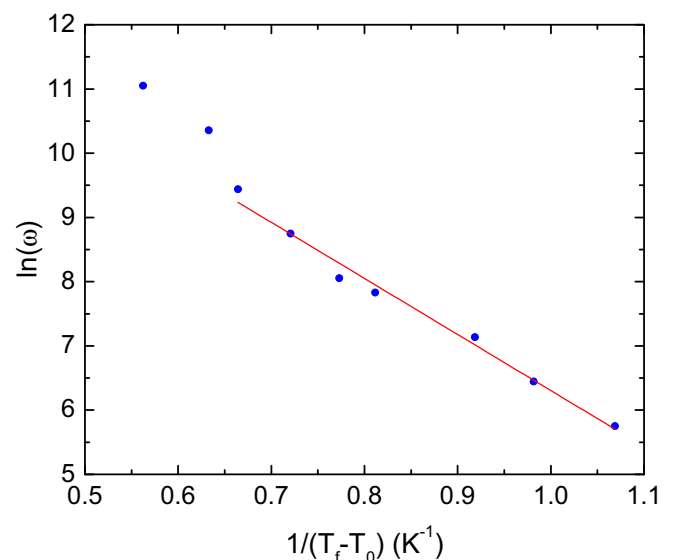
FIG. 7. (Color online) Natural logarithm of frequency dependence of the cusp in the real susceptibility for sample 1 as a function T_f using a value of $T_0 = T_f(0) = 11.52$ K. The line is a fit to the data using the Vogel-Fulcher law [Eq. (6)].

TABLE III. Parameters calculated from the AC susceptibility of two separate samples of Ni(TCNQ − D$_4$)$_2$.

Parameter	Sample 1	Sample 2
T_0 (K)	11.52(4)	13.94(4)
φ	0.0315(4)	0.023(2)
E_a/k_B (K)	8.7(4)	8.5(5)
$\omega_0/2\pi$ (MHz)	0.53	1.05

TABLE IV. Parameters from the analysis of the imaginary component of the susceptibility for the two separate samples.

Parameter	Sample 1	Sample 2
T_{f0} (K)	9.0(2)	11.2(2)
φ	0.059	0.051
E_a/k_B (K)	19(2)	21(2)
$\omega_0/2\pi$ (MHz)	17.6	18.0

It is found that $E_a/k_B = 8.7 \pm 0.4$ K and $\omega_0/2\pi = 0.53$ MHz which is known as the attempt frequency, and it should be noted that this is of a similar value to that observed in the zero-field μSR data that will be discussed in a later section. Also, it should be noted that the linearity of the plot in Fig. 7 improves as T_0 is reduced, but the values of E_a and ω_0 rapidly deviate from what is physically sensible.

A separate sample of Ni(TCNQ − D$_4$)$_2$, sample 2, was synthesized using the same method as was adopted for sample 1 and the AC susceptibility measured to compare with the previously discussed data. The results were analyzed in a similar method to the sample discussed above and summarized in Table III.

The results obtained from sample 2 are slightly different from those of sample 1 indicating that the method of material synthesis is not completely reproducible. One significant result is the reduction in φ, which is not accounted for by the error, which means that this sample shows a weaker frequency dependence. The frequency dependence (φ) has changed from sample 1 to sample 2, and this implies the two different samples have different degrees of magnetic disorder. The two samples also differ in T_0 where the previous sample has a lower value for the freezing temperature, again supporting the idea that the samples have differing degrees of magnetic disorder.

The imaginary component of the susceptibility is shown in Fig. 8 and appears at temperatures below about 15 K in accordance with the frequency-dependent peak in χ'. It is a very weak effect only in systems where the relaxation process can decouple the spins from the lattice, such as with hysteresis [12].

The imaginary susceptibility of Ni(TCNQ − D$_4$)$_2$ shows a very weak frequency dependence, and the broadness of the transition may suggest that there is a distribution of relaxation times. However, the imaginary susceptibility is parameterized using the Vogel-Fulcher method in a similar manner to the real component of the susceptibility, and the results from samples 1 and 2 are shown in Table IV.

We note that VF parameters obtained for both χ' and χ'' differ. This is likely to be a consequence of the fact that the peak in χ' is related to the result of the onset of the imaginary or lossy component of the magnetism and corresponds to the emergence of the hysteretic behavior observed in the DC magnetization measurements. Therefore it is likely that this effect is strongly coupled to the ferromagnetic behavior of the sample. The peak in χ'' is probably associated with the magnetic relaxation process associated with energy barriers arising from the interactions between the nanograins of Ni(TCNQ − D$_4$)$_2$. In fact peaks in both χ' and χ'' vs frequency are seen in ferromagnetic nanoparticulate systems where there is a broad distribution of particle sizes and thus relaxation times. When these are magnetically frozen out (or blocked) one observes a drop in the susceptibility, both real and complex, which is a function of frequency [46–48]. Within the Ni(TCNQ − D$_4$)$_2$ system we may be seeing something similar, and we may deduce that the nanograins have a broad size distribution and a peak in the susceptibility shows that the measurement is sensitive to a cluster size distribution that is within the distribution of relaxation time scales of the order of the AC susceptibility measurements. Moreover, the typical values obtained for φ (Tables III and IV) would suggest that such ferromagnetic clusters are interacting with one another.

Note that the two samples (1 and 2) show different time scales for the attempt frequency, with the second sample having a much slower dynamical component which may be a result of the shift in T_f. The fact that it has not been possible to reproduce samples with a similar T_f suggests that the synthetic method does not produce an exact stoichiometric material, with the same nanostructure, every time.

2. Heat capacity

Heat capacity measurements were conducted on a sample of Ni(TCNQ − D$_4$)$_2$ to complement the susceptibility data. The results are shown in Fig. 9, and it is noticeable that no significant feature is associated with the bulk ferromagnetic transition at 20 K.

At low temperatures (i.e., as $T \rightarrow 0$ K), where the results of the previous sections suggest glassy behavior is expected to dominate the material's properties, one might expect that there is a change in the data where the nonzero heat capacity

FIG. 8. (Color online) χ'' vs temperature for a fresh sample of Ni(TCNQ − D$_4$)$_2$.
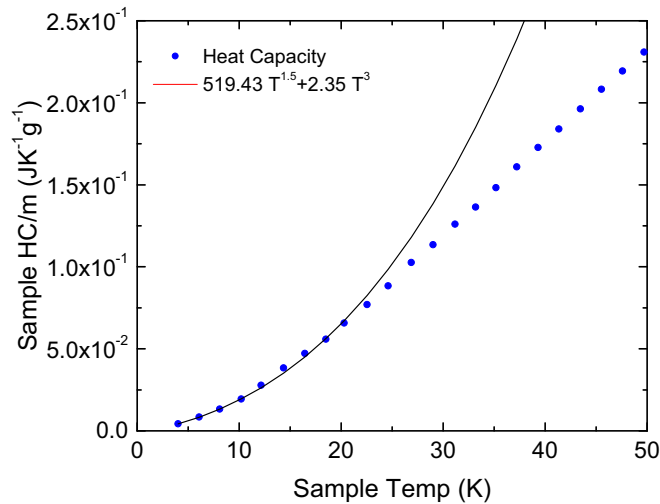
FIG. 9. (Color online) Heat capacity of Ni(TCNQ − D$_4$)$_2$. The solid line is a fit to the low temperature points using Eq. (11).

signifies that there is residual entropy within the system which could probably be from magnetic disorder. However our heat capacity data can be interpreted differently as, although at 2 K the heat capacity has not reached zero, the analysis performed (given below) provides a reasonable fit without including an offset term, indicating that the heat capacity of the system may in fact go through the origin at absolute zero.

Assuming that the material is a 3D ferromagnet, the data are fitted to a function containing a term describing contributions from spin waves ($\propto T^{\frac{3}{2}}$) and the lattice ($\propto T^3$),

$$C = \alpha T^{1.5} + \beta T^3, \tag{7}$$

which describes the observed heat capacity only at very low temperatures (2 K < T < 12 K) where $\alpha = 519 \pm 7 \, \mu\text{JK}^{-\frac{5}{2}}\text{g}^{-1}$ and $\beta = 2.3 \pm 3 \, \mu\text{JK}^{-4}\text{g}^{-1}$. More generally, spin waves contribute to the magnetic heat capacity with the form [49],

$$C \propto T^{d/n}, \tag{8}$$

where d is the dimensionality, and $n = 2$ for a ferromagnet and 1 for an antiferromagnet. However, the fit to the data in Fig. 9 supports a temperature dependence of $T^{\frac{3}{2}}$ leading to the values $d = 3$ and $n = 2$. (An alternative method may be used to analyze the temperature dependence of the heat capacity [50,51] which involves a polynomial fit to higher temperature C values; see the Supplemental Material [31]). We note that a T^3 implies a 3D lattice contribution to the low temperature heat capacity of the Ni(TCNQ − D$_4$)$_2$ sample which consists of nanograins. However, there have been reports of other nanostructured materials exhibiting such a temperature dependence, though the measured Debye temperatures did not correspond to bulk values [52,53]. This suggests that, in Ni(TCNQ − D$_4$)$_2$, there is strong enough coupling between the nanograins to allow long wavelength lattice vibrations to contribute to the heat capacity.

Considering the magnetic contribution to the heat capacity data, it is also possible to estimate the exchange energy of the magnetic ions using the relationship [42] (assuming a simple cubic structure)

$$C_{\text{mag}} = \left(\frac{0.113R}{m_r}\right)\left(\frac{k_B T(S_1 + S_2)}{4 J_{\text{ex}} S_1 S_2}\right)^{\frac{3}{2}}. \tag{9}$$

Here R is the universal gas constant, and m_r is the molar mass of the compound. Using $S_1 = 1$ and $S_2 = \frac{1}{2}$, an estimate of the exchange integral is found to be $J_{\text{ex}}/k_B = 1.83(2)$ K, which is similar to the exchange energy calculated from the magnetization data. As discussed previously regarding Bloch's law, if a smaller value of the coefficient of the $T^{3/2}$ is also obtained with nanograined Ni(TCNQ − D$_4$)$_2$, then that value of J_{ex} obtained from the analysis of C (and that obtained from M vs T data) may be underestimates of the correct value. Nevertheless, there is a clear consistency between the values of J_{ex} obtained from T_C, low temperature magnetization, and heat capacity.

C. Muon spin relaxation study

μSR provides an ideal experiment for studying weak magnetism on both a local and a long range scale [54]. Within the experiment, spin polarized muons are implanted within the sample, and the asymmetry in their forward and backward decay is measured as a function of time, which can provide information on the internal field at the muon site as well as magnetic fluctuations within the time scale of the experiment (generally on the MHz time scale). μSR experiments were performed on Ni(TCNQ − D$_4$)$_2$ where the deuteration of the compound was an advantage as it provided an environment with lower nuclear fields compared to that of the protonated material. This meant that the only important nuclear spins that would contribute to the depolarization of the muon were those of the nitrogen atoms. Neutral TCNQ has been studied using muon spectroscopy where a radical with an 80 MHz coupling constant was observed which corresponds to coupling of the muon to the nitrogens at the end of the molecule. In reduced TCNQ it may be possible to observe bonding of the muon to the aromatic ring which would have a higher hyperfine coupling [55]. Thus, although deuterium has a nuclear magnetic moment, because it is smaller than that of ^{14}N and given the suspected stopping site of the muon, it can be effectively ignored. Since positive muons are implanted into the material, one expects the muon to stop next to areas of negative charge that, within our sample, would be sites close the TCNQ where the anion radical is stabilized, i.e., the cyano groups at one end of the TCNQ molecule. However, the magnetic environment of the muon is complicated and so the muon will be sensitive to both the nuclear magnetism on the nitrogen atoms and also the electronic magnetism below T_C. Note that some of the results presented here have been briefly reported previously [56].

1. Zero field μSR

ZF experiments were conducted on a fresh (< 1 month old) sample of Ni(TCNQ − D$_4$)$_2$. The same sample was used for the neutron diffraction experiment on D1B, and since there is evidence of weak magnetic Bragg peaks one would expect the muons to be sensitive to this magnetism.
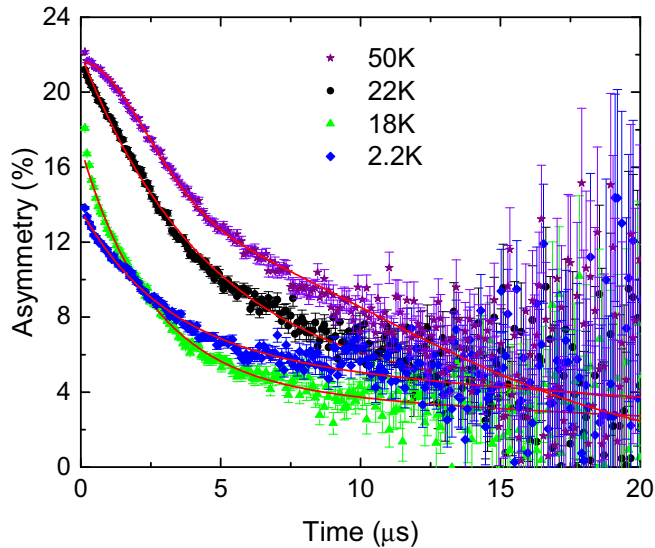
FIG. 10. (Color online) ZF μSR raw asymmetry data at selected temperatures above and below $T_C \approx 20$ K.

The raw data from the ZF experiment at selected temperatures are shown in Fig. 10, and it is clear that the relaxations are qualitatively different above and below the Curie temperature. At 50 K (i.e., $T > T_C$) the data must be fitted using a sum of two Gaussian functions [see Eq. (10)] which is likely to be describing the relaxation due to the static nuclear fields on the ^{14}N atoms for both components 1 and 2,

$$G(t) = A_1 \exp\left(-\sigma_1^2 t^2\right) + A_2 \exp\left(-\sigma_2^2 t^2\right) + A_{\mathrm{Bg}}. \quad (10)$$

Here A_i is the asymmetry associated with the ith muon stopping site, A_{Bg} is the baseline which accounts for muons that are relaxing in the silver sample holder or cryostat, and σ_i is the relaxation parameter that is dependent upon the local magnetic field at the ith muon stopping site.

The fact that the relaxation at 50 K cannot be modelled simply using a single Gaussian (see Table V for values of fitting parameters) suggests that there are two muon stopping sites within the sample. These may be next to the negative charge on the cyano groups at the end of the TCNQ moiety and also above or below the aromatic ring on a TCNQ molecule where there is significant $\pi -$ electron density. At these different stopping sites the magnitude of internal nuclear field strength will be different as it depends on the distance from the nuclear moments. So each muon will experience a different net local field, and their relaxations will differ corresponding to different

TABLE V. Parameters from a fit to the high temperature μSR data. The background was fixed at 2.5% and was held constant throughout the analysis; the errors are given in brackets.

Parameter	Value
A_1 (%)	11.3 (0.1)
A_2 (%)	7.7 (0.1)
A_{Bg} (%)	2.5
σ_1 (μs^{-1})	0.081 (0.001)
σ_2 (μs^{-1})	0.327 (0.004)

values of σ. Since $\sigma_1 < \sigma_2$ this means that the field distribution experienced by μ_1^+ is larger than that for μ_2^+. At the site where the muon is coupled to the nitrogen the distribution of nuclear fields will be larger than if the muon was coupled to the aromatic ring, therefore we may have a case where muons are coupled to both the ring and the cyano groups. However it could be that two different muons are implanting to two different sites where the magnetic behavior differs, i.e., in the center and edge of a magnetic cluster, which will be discussed in more detail later.

As T approaches T_C from above, the relaxation has an increasingly non-Gaussian form and is closer to a simple exponential for $T < T_C$. One assumes that the electronic magnetism has a larger contribution to the muon relaxation as they become quasistatic, and so when going through T_C the overall magnetism of the material dominates the muon relaxation signal. Note that no oscillatory signal, a characteristic of the presence of magnetic order, is observed and, in fact, in this regime the data were fitted using a summation of two single exponential relaxations,

$$G(t) = A_1 \exp(-\lambda_1 t) + A_2 \exp(-\lambda_2 t) + A_{\mathrm{Bg}}. \quad (11)$$

Here λ_i is the relaxation parameter that again is proportional to the local internal magnetic fields experienced by the muons at the ith site. Following the analysis of the 50 K ZF μSR data, the two relaxations observed close to or below T_C account for two different muon stopping sites. The baseline (A_{Bg}) was kept fixed at 2.5% as it is not expected to change as a function of temperature. The value of λ_2 was kept fixed at 0.03 μs^{-1} and describes the tail of a relaxation that is outside of the time window of the measurement and not accounted for in the baseline. If there is indeed a relaxation that is outside of the EMU time window, this may imply that at one muon stopping site the internal fields are at such a high value that the implanted muons are dephased very quickly and we cannot detect their relaxation. It should be noted that Eq. (11) was used to fit to the higher temperature data as this allowed some form of parametrization, though above the critical region this may not be the most physically relevant description.

The asymmetries of components 1 and 2 (A_1 and A_2, respectively) are shown in Fig. 11 where A_2 (blue triangles) is showing a dramatic change at 19 K that corresponds to the ferromagnetic transition. As the sample approaches the magnetic phase transition from a higher temperature, the fluctuating spins begin to order and the magnitude of the internal field increases. If the muons experience a high field, then they are dephased very quickly and thus one sees a missing fraction upon entering the ordered phase, the static field being large enough to depolarize the muons outside of the EMU instrument's time window. The asymmetry of component 2 is well coupled to the transition that suggests it has a relationship to the electronic magnetism within the sample. As $T \to 0$ this contribution increases which again suggests that it is due to the increased magnetic order within the material as the fluctuations will freeze out below T_C, however the exact nature of this relaxation cannot be determined from our data.
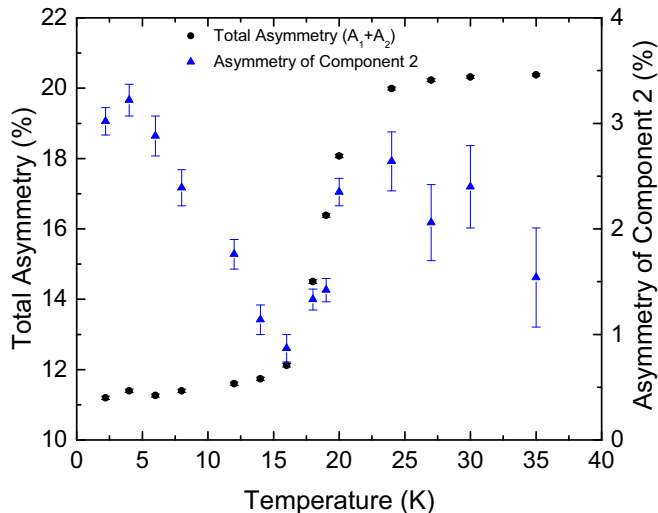
FIG. 11. (Color online) ZF total asymmetry and the second component asymmetry (A_2).

The ZF relaxation parameter, λ_1 of the first component, shown in Fig. 12, is related to the spread of internal fields (Δ) and the rate of fluctuation (ν) of the electronic moments as in the fast fluctuating limit $\lambda \propto \Delta^2/\nu$. From the data it is clear that the sample goes through a transition at $\sim$19 K where the fluctuating magnetic moments slow down and the system enters an ordered phase (on the time scale of the muon). The apparent plateau at 14 K may be real and indicates that there is a more complex magnetic behavior (i.e., another peak in λ_1) present, however more data is needed to confirm this conclusion.

Below 6 K the value of λ_1 begins to increase rapidly, and from the magnetization data shown in Fig. 2 one can see that the ZFC curve changes slope at about the same temperature. The increase in the muon relaxation at these low temperatures indicates that the system may be approaching another magnetic phase transition below 2 K, our lowest
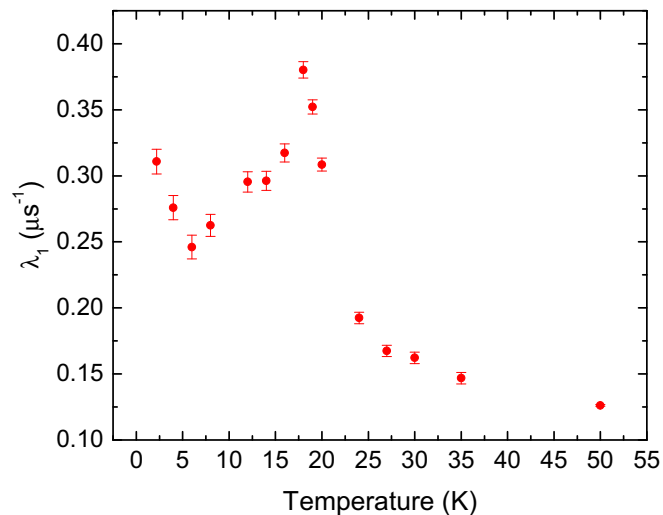
accessible temperature. Below this temperature it may be that the system adopts, say, a superspin glass state due to interactions of the individual ferromagnetic regions. However one cannot rule out the possibility of another exchange mechanism becoming influential at very low temperatures and modifying the magnetically ordered state. For example, TCNQ-TCNQ interactions, which are known to be present in other 1:2 TCNQ based materials [57], which would again change the field distribution and electronic fluctuations thus leading to observable changes in λ_1.

2. Longitudinal field μSR

Longitudinal field measurements allow decoupling of the components within the muon relaxation, i.e., by application of a field one can repolarize muons that are dephased by the nuclear moments on the nitrogen atoms. It is also possible to decouple static magnetism and to study the dynamics within a system.

Although the sample was deuterated, minimizing the possibility of muon hyperfine coupling to the protons on the TCNQ ring, coupling between the muon and the nuclear moment on the nitrogen nuclei is likely as suggested by ZF measurements at 50 K. To decouple this nuclear contribution a longitudinal field (LF) ($\leqslant$ 450 mT) was applied which acts to repolarize muon spins. We find that an optimal LF for decoupling the nuclear component is 5 mT which will be discussed in more detail later. At high fields one might expect to repolarize all the muons spins, including those relaxed by static local fields which are electronic in origin, so a full fraction is recovered. However, this was not the case up to 20 K where the effect is more extreme at lower temperatures (see Fig. 13). At 2 and 6 K and 450 mT LF a 21% total asymmetry was reached (a full fraction on the EMU instrument being taken as $\sim$23%) which suggests that even at these high LF values there is a significant dynamical contribution to the magnetism within the system. In fact, at an LF above 10 mT

FIG. 12. (Color online) ZF relaxation parameter of component 1 from fits to the raw data using Eq. (11).
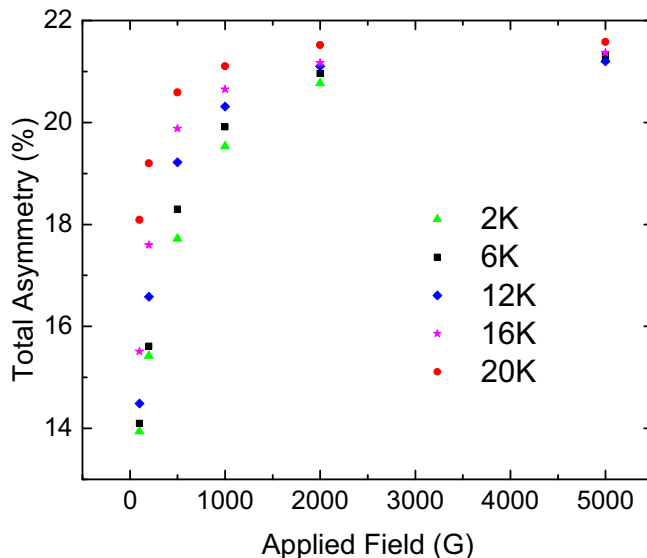
FIG. 13. (Color online) Total asymmetry as a function of applied LF where $B \geq 10$ mT.
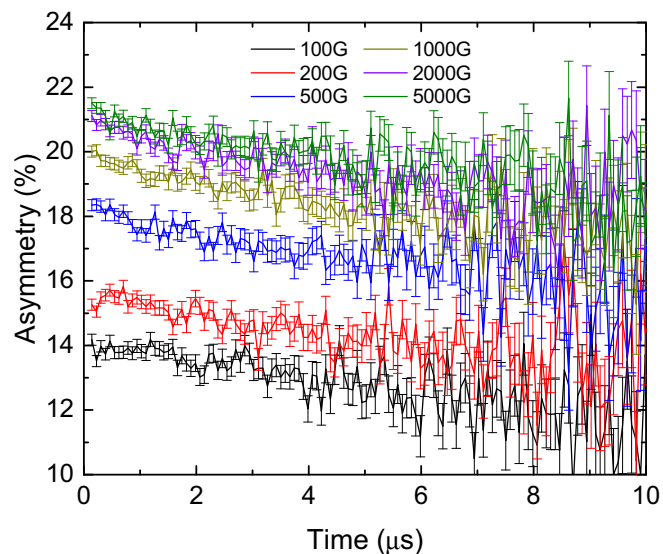
FIG. 14. (Color online) The asymmetry at 6 K at different LF values. From the data one can see the relaxation is very small and is essentially the same at each LF, and only the asymmetry is changing.

FIG. 15. (Color online) Time dependent μSR spectra with a 5 mT LF where there is a complete decoupling of the nuclear component and the emergence of a heavily damped oscillation as T_C is approached. The lines are fits to the data using Eq. (3).

a single exponential relaxation function was fit to the data where $\lambda_{LF} = 0.146 \pm 0.018\ \mu s^{-1}$ for all temperatures and at all field values; the raw data are shown in Fig. 14 at 6 K. There is little difference between the relaxation rates at different temperatures as the LF is ramped, the only field dependent change being in the total asymmetry.

Since the λ_{LF} value could be fixed, it means that the same relaxation process is dominant at all temperatures and supports there being significant dynamical fields within the system. The fact that there is a dramatic change in the LF data at ~10 mT indicates that the spread of internal fields in the sample, which acts to depolarize the muons spins, is around this magnitude.

In an LF of 5 mT a markedly different relaxation was observed from that of the ZF measurements as shown in Fig. 15. The best fits to the data were obtained using a heavily damped oscillatory function that captured the behavior at very short times:

$$G(t) = A_1 \exp(-\lambda_1 t) \cos(\omega t + \phi) + A_2 \exp(-\lambda_2 t) + A_{Bg},$$

(12)

where ϕ (fixed at 0.12) is the phase component. Similar to the ZF fits, the value of λ_2 was fixed at 0.03 μs^{-1} and the background asymmetry was set at 2.5%. The oscillation frequency was also fixed at 0.6 MHz (~4.4 mT) which is related to the field experienced by the muon by $\omega = \gamma_\mu |\mathbf{B}|$, where γ_μ is the gyromagnetic ratio of the muon. The damped oscillation is an indication that there are internal fields, larger than the applied LF, that are transverse to the initial muon spin polarization. The value that is obtained for the frequency will be a vector sum of the internal fields experienced by the muon, explaining why the value of $\mathbf{B}_{int}$ is lower than the applied LF. The frequency calculated may relate more to the distribution of the internal static fields, where the applied LF has provided a magnetic field that is larger than that experienced by the muon from the fluctuating moments near the stopping site. The fact that the oscillation is dephased quickly (i.e., is heavily
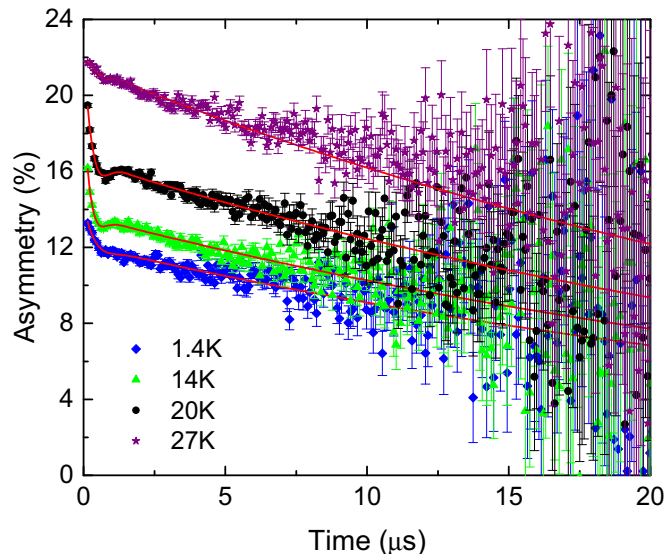
damped) suggests that the muon is experiencing a significant distribution of static fields that may result in a relatively high precession frequency that cannot be measured on the μSR instrument's time scale.

The values of λ_1 for the LF data shown in Fig. 16 are an order of magnitude larger than those of the ZF results indicating a very fast relaxation of the muon spins. However, what is striking is that, although the low temperature rise in λ_1 is still present, the higher temperature peak is at 12–13 K, which is at a similar temperature to the divergence of the ZFC/FC magnetization curves shown in Fig. 2. It is therefore likely that, in an LF of 5 mT, the muons are sensitive to a different relaxation process which may be due to the
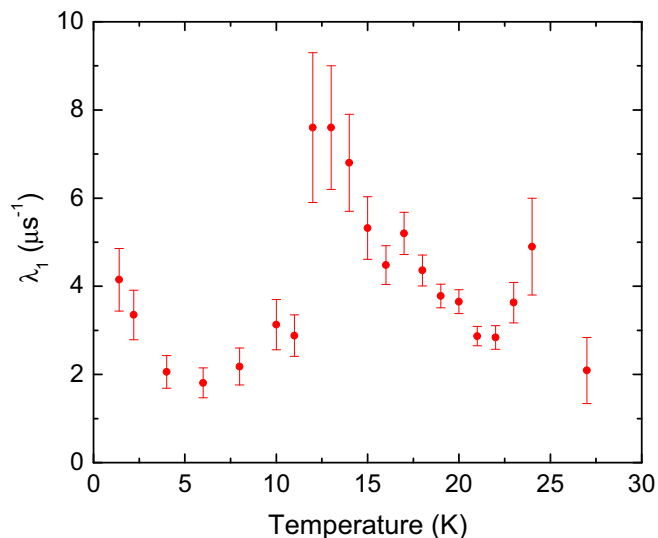
FIG. 16. (Color online) 5 mT LF relaxation parameter λ_1, obtained from Fig. 15, as a function of temperature.

ferromagnetic particles that have a coercive field larger than 5 mT but smaller than 10 mT as the evidence of an oscillation is not present in the LF 10 mT spectra, which indicates a much larger coercive field than that from the magnetization measurements. This may be due to the muons being sensitive to a range of cluster sizes where one sees a dampening of the relaxation at 10 mT, which may correspond to the collapse of hysteresis in larger magnetic clusters. The peak in λ_1 at 25 K may not be physically meaningful as we are above T_C, and what this relaxation is capturing is the very fast relaxation at very short times. When looking at the magnetization data in Figs. 2 and 3, there is nothing to suggest that we should observe a feature above T_C. In fact what we might be observing is the external applied field magnetizing the sample within the critical region which would distort the field distribution and fluctuation rates.

This again supports the conclusion for the LF data that the internal fields are approximately 10 mT. The precession frequency of 0.6 MHz is not indicative of a response of the muon to a purely electronic component. Generally very low frequencies (or small internal fields) are from the coupling of the muon to a nuclear component, however if the muon stopping site is far away from the static fields then the dipolar coupling between the muon and magnetic moment will drop off as $1/r^3$ and thus the field at the muon site may be weak which could result in a low frequency. It may be that this fit, however, is more empirical or phenomenological with the slow frequency capturing the dip in the data and the two Lorentzian relaxations describing the two distinct magnetic components. The total asymmetry (see Fig. 17) also shows a large change at approximately 12 K though A_2, for 5 mT LF, shows a coupling to the ZF magnetic transition (20 K) indicating that this component has also undergone little change with a small applied field (see Fig. 11 for comparison). It is therefore A_1 that dominates the muons relaxation and is affected most by the applied LF. Thus with an applied field of 5 mT we are not only repolarizing muons that are dephased by the nuclear magnetic fields but also perturbing the magnetism of the

FIG. 17. (Color online) 5 mT LF relaxing asymmetry and 2nd component asymmetry (A_2). Both parameters were obtained from Fig. 15.

sample. Therefore this is why λ_1 is sensitive to the hysteretic behavior of the material, where at 12 K we are observing a freezing out of magnetic fluctuations associated with the ferromagnetic state. It should be noted that the sample was cooled in the absence of an applied field, and this is supported by our ZFC magnetization data where we see a divergence of the ZFC/FC curves that correspond to hysteric behavior at approximately 15 K.

IV. DISCUSSION

The $M(\text{TCNQ})_2$ samples are believed to be crystalline materials and, in the case where $M = \text{Ni}$, we have shown that the deuterated analogues show diffraction peaks that correspond to the existence of an ordered crystal. For the Ni sample the diffraction data has not yielded any firm conclusions on the atomic structure, and the crystallinity appears to be weak and have a short coherence length. The SEM images show that micron-size particles are synthesized within the deuterated sample. However, PXRD data, analyzed using the Scherrer equation, suggested that these particles consist of grains or crystallites, each with an average size of approximately 30 nm.

The magnetic data show some very interesting results where the sample is shown to behave like a ferromagnetic material which at low temperatures enters an ordered phase that can be described by a Bloch's law indicating the existence of a classical 3D spin wave system. The resulting $T^{\frac{3}{2}}$ dependence of the magnetization as a function of temperature only occurs well below the transition. This is supported by the heat capacity data where again the low temperature data can be shown to also follow a $T^{\frac{3}{2}}$ function as well as a small contribution from the lattice which goes as T^3. This is quite different from the observed behavior of $[\text{MnTPP}]^+[\text{TCNE}]^- x(1,3$-dichlorobenzene) where the cluster glass regime is believed to show a 1D to 2D evolution through T_g [19–21].

Analysis of the AC susceptibility data shows that the sample is likely to have a glassy component associated with the transition where the values of φ do not agree with that of an ideal superparamagnet and are closer to the values of the canonical spin glasses [12] or interacting superparamagnetic particles. The ferromagnetic transition in the magnetization data, however, does not show any resemblance to a spin glass where one expects the FC curve to flatten out where the moments freeze into one of the metastable ground states, suggesting that the transition and the glassy nature of the material may be due to different things. One possible model is that, within the sample, there are short range interactions, similar to that within $V(\text{TCNE})_x$ [25], where the exchange mechanism is through a random anisotropic pathway leading to disorder driven magnetism. In such a model, the magnetic regions or clusters (of size 30 nm) undergo a percolative transition to a ferromagnetic phase as $T \rightarrow 0$. As T decreases through T_C, the coherence length of these magnetic clusters grows, and ultimately interaction between these clusters leads to a glassy ferromagnetic state which can lead to a complex magnetic ground state. It should be noted that this infinite cluster formed at $T = 0$ K is effectively made up of many randomly frozen smaller clusters.
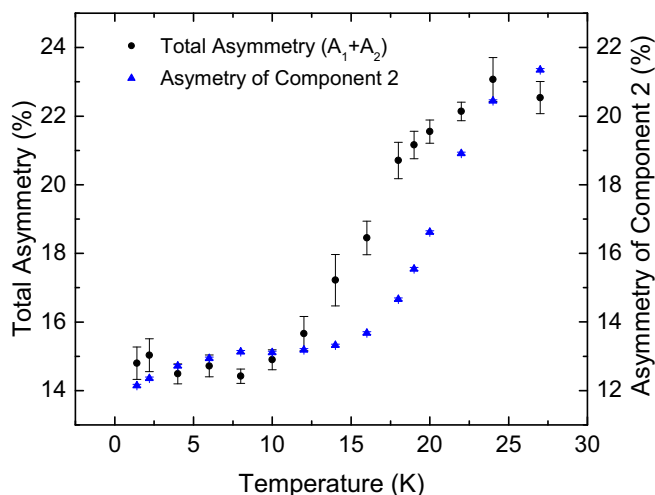
This model is similar to that proposed to describe the inorganic disordered perovskite, $La_{1-x}Sr_xCoO_3$ (LSCO). In the undoped form $LaCoO_3$ undergoes a temperature driven metal-insulator transition which is due to a spin state transition of the Co^{3+} ion, however there is some ambiguity as to whether at high temperatures this shows an $S = 1$ (intermediate) or $S = 2$ (high spin) state [58]. Doping with Sr^{2+} ions not only creates holes but also induces disorder within the system. Hole doping the material induces an insulator-to-metal transition with increasing x. At low doping, the magnetism of the insulating phase shows characteristic spin glass behavior, however when $x > 0.18$ this magnetism shows characteristics of a 3D ferromagnetic metal. The insulator-metal transition is believed to be percolative and is associated with magnetoelectronic phase-separated regions [59]. At low x the magnetism is dominated by the Co^{3+} antiferromagnetic superexchange interactions, however increased doping leads to an increased number of Co^{4+} ions which drives the local interactions into a double exchange ferromagnetic state leading to the aforementioned magnetic clusters. The spin glass behavior is due to the competing ferromagnetic and antiferromagnetic interactions within the systems, where irreversibility is also observed in the ZFC/FC data. The AC susceptibility data also show a frequency dependence of the transition even in the ferromagnetic phase which is clear evidence of spin glass freezing. The LSCO system may be a parallel to the studied $Ni(TCNQ - D_4)_2$ samples, where we are also observing very strong evidence for ferromagnetic behavior in both the magnetization and heat capacity measurements. However the AC susceptibility appears to show some characteristics of spin glasslike behavior, but this may be due to interacting superparamagnetic particles.

The μSR data showed more insight into the glassy component associated with the magnetism. An interpretation of the different muon stopping sites, along the ferromagnetic glassy behavior observed in bulk measurements, is that we are observing a relaxation from one muon that is stopping in the center of a large particle and another that may be sensitive to the surface or walls between the particles in a system like a cluster glass. If a muon were to stop in the center of a particle, the internal fields may be very large which would depolarize the muon too quickly and outside of the measurable time window at ISIS. If this were the case we would expect to see a 1/3 tail in the asymmetry that would correspond to the magnetic component aligned along the z direction, or initial muon polarization. Ultimately the fixed λ_2 values may be the late time of this relaxation from the muons experiencing a very large internal field. A 1/3 tail is not obvious in the raw data as there is a continuous decay as time increases down to the baseline and hence another relaxation process dominates, which may be from muons that are stopped close to the surface or wall of the particles where the internal fields may be much weaker. The fact that λ_1 peaks at T_C in ZF shows that these muons are sensitive to the bulk magnetization of the ferromagnetic component when the material is entering an ordered magnetic phase. However, the LF sweeps show that there is a significant dynamical component present, and the muons are likely to experience motional narrowing by these fast fluctuating local fields with no applied field.

Note that Clérac *et al.* [13] concluded that the $M[TCNQ]_2$ system exhibited a magnetically glassy state below T_C. However, this μSR investigation suggests that the magnetic glassiness (at $T = 5$ K) may be due to the interaction of the magnetic particles, where the system is behaving similar to a supperspin glass [60] or a cluster glass. Here the dipolar fields from each individual magnetic cluster attempt to align their neighbors to minimize the energy, which may also lead to an element of frustration as can be seen in spin glasses. There is no evidence from the μSR data that there is a glassiness associated with the ferromagnetic transition at $\sim$20 K. The presence of a spin glass would be indicated by a characteristic decay where a stretched exponential could be fit to the data suggesting a range of time scales of the relaxation of the magnetism similar to that observed in spin glasses [61], where the line-shape parameter tends to 0.33 upon going through T_f. Such a decay was not observed in μSR measurements of $Ni(TCNQ - D_4)_2$. Therefore there are two distinct temperatures, a ferromagnetic transition ($T_C = 20$ K) and possibly a magnetic freezing temperature ($T_f = 5$ K) which is unlikely to be related to magnetic frustration at an atomic level.

Application of a field of 5 mT results in a heavily damped oscillation being observed in the μSR data, where the nuclear field component of the muon relaxation has been decoupled. These oscillations may be revealing the underlying magnetic ordering, but since a standard Kubo-Toyabe relaxation function does not describe the data it is likely that the application of a 5 mT field is actually affecting the sample itself and disturbing the internal magnetism. This may act to slow the magnetic fluctuations within the material at the two stopping sites identified in the ZF measurements. In fact applying a field would also be expected to align the large spins of the clusters and also the magnetic moments within the walls between these clusters/particles. The increase in the values of λ_1 indicates that the application of the field has suppressed a slow relaxation. This faster relaxation rate is sensitive to both a transition with a peak at 15 K, which is similar to both the divergence of the ZFC/FC magnetization curves and the onset of the time dependence of the AC susceptibility, and a freezing temperature below 5 K which seems unaffected by the 5 mT LF.

An explanation of the μSR results presented so far may be obtained by considering the inorganic system, $GdPO_4$. A bulk sample was studied using μSR where a static component was observed that shows a T_C of approximately 1 K. However when nanoparticles are made of $GdPO_4$ the muon relaxation observed has both a static and dynamical component to it. The static component shows a reduced T_C which is expected with nanoparticulate systems [62] and is modelled by a static KT function. The dynamic component persists down to 40 mK and is best described by a single exponential relaxation where below 0.7 K bulk magnetic ordering is observed. The main difference is that there is another peak in λ at a lower temperature where the parameter increases at 0.4 K which Evangelisti *et al.* have attributed to a spin freezing effect where the nanoparticulate system moves into a quasistatic regime from interparticle interactions [63]. $GdVO_4$ nanoparticles were also synthesized where similar behavior was observed, however the spin freezing peak in λ was much less pronounced which is suggested to be due to more magnetic

disorder within this quasistatic regime [63]. This may support the similar behavior seen within the Ni(TCNQ $- D_4)_2$ system where the increase in the ZF λ_1 parameter is attributed to a spin freezing temperature or the material entering a quasistatic regime. However from the SEM images it is likely that the Ni(TCNQ $- D_4)_2$ material is made of micron-sized particles consisting of nanocrystallites.

Another comparable inorganic system is that of La$_{0.7}$Pb$_{0.3}$(Mn$_{1-x}$Fe$_x$)O$_3$ (LPMFO) where $0 \leq x \leq 0.2$ [64]. Within this system there are two forms of exchange that compete, and as x increases this increases the disorder within the material which pushes down the critical temperature. When $x = 0.2$ the FC magnetization data shows a flat top below T_C which is consistent with a spin glass or in this case a cluster glass. μSR measurements on an undoped sample show changes in the relaxation and asymmetry as the sample goes through T_C. However, when doped with Fe the behavior changes, and not only is a peak that is associated with the transition observed, but a second peak appears at lower temperatures which is attributed to spin freezing of magnetic clusters. As the disorder is increased within the system both T_C and the spin freezing peak shift to lower temperatures, and ΔT between them increases. Below this spin freezing temperature the moments go from a dynamic to a static disordered regime where ferromagnetism is observed through a percolation type behavior. This model fits in more with the picture of Ni(TCNQ)$_2$, where we believe disorder may play an important role in producing the magnetic properties of the system. If within Ni(TCNQ)$_2$ there are defects that act to pin domain boundaries, then we may be observing the bulk magnetic transition in the center of these domains or magnetic clusters. The ferromagnetism is then induced in the whole material by a percolation transition, and below 5 K the material enters a static disordered regime whereby the magnetic clusters can interact as the spin fluctuations, which are measured in ZF by λ_1, freeze out. Similar spin freezing effects are seen within Ca$_3$Co$_{2-x}$Mn$_x$O$_6$ with $x = 1$, which behaves like a cluster glass, and the value of λ increases rapidly as the temperature is cooled through the spin freezing transition where the magnetic clusters lock into a random configuration and the moments become quasistatic [65].

V. CONCLUSION

Within this paper we have presented a detailed study of the metal-organic magnetic material Ni(TCNQ $- D_4)_2$, where a variety of techniques have been employed to attempt to pick apart the complex magnetic behavior. The sample was shown to behave as a 3D ferromagnetic system, where the magnetization and heat capacity show the classic spin wave behavior, though one with a granularity of size 30 nm. Moreover, neutron scattering results exhibit very weak magnetic peaks. AC susceptibility suggests that there is a glassy component to the magnetically ordered state upon going through T_C, but μSR measurements do not support the presence of a spin glass state, at least down to 2 K. Moreover, the μSR results suggest the presence of magnetic fluctuations well below the Curie temperature of 20 K. Such observations may be consistent with either a superspin glasslike behavior arising from interacting superparamagnetic regions of the material or perhaps inhomogeneous ferromagnetic regions interacting to produce a cluster-glass-like state. Indeed, the muon relaxation shows two transitions, one at approximately 20 K and one below 6 K, which is evidence that the magnetically ordered and glassy states are separate. Overall we have shown that this metal-organic magnet is comprised of regions of ordered clusters with significant disorder that results in a magnetic cluster glass behavior. This explains the glassy nature of the material, however it should be stressed that a phase pure sample without the disorder may show interesting magnetic properties that should be explored further.

[1] S. J. Blundell and F. L. Pratt, J. Phys.: Condens. Matter **16**, R771 (2004).

[2] J. S. Miller, Chem. Soc. Revs. **40**, 3266 (2011).

[3] J. S. Miller and A. J. Epsteinn, Angew. Chem., Int. Ed. Engl. **33**, 385 (1994).

[4] J. S. Miller, Pramana **67**, 1 (2006).

[5] D. S. Acker and W. R. Hertler, J. Am. Chem. Soc. **84**, 3370 (1962).

[6] J. S. Miller, J. H. Zhang, W. M. Reiff, D. A. Dixon, L. D. Preston, A. H. R. Jr., E. Gebert, M. Extine, J. Troup, A. J. Epstein, and M. D. Ward, J. Phys. Chem. **91**, 4344 (1987).

[7] A. H. R. Jr., L. D. Preston, J. M. Williams, S. W. Peterson, G. A. Candela, L. J. Swartzendruber, and J. S. Miller, J. Am. Chem. Soc. **101**, 2756 (1979).

[8] J. S. Miller, A. H. R. Jr., E. Gebert, J. J. Ritski, W. R. Salaneck, L. Kovnat, T. W. Cape, and R. P. V. Duyne, J. Am. Chem. Soc. **101**, 7111 (1979).

[9] W. E. Broderick, D. M. Eichhorn, X. Liu, P. J. Toscano, S. M. Owens, and B. M. Hoffman, J. Am. Chem. Soc. **117**, 3641 (1995).

[10] M. L. Taliaferro, T. D. Selby, and J. S. Miller, Chem. Mater. **15**, 3602 (2003).

[11] J. S. Miller, J. C. Calabrese, H. Rommelmann, S. Chittipeddi, J. H. Zhang, W. M Reiff, and A. J. Epstein, J. Am. Chem. Soc **109**, 769 (1987).

[12] J. A. Mydosh, *Spin Glasses: An Experimental Introduction*, 1st ed. (Taylor and Francis, London, 1993).

[13] R. Clérac, S. O'Kane, J. Cowen, X. Ouyang, R. Heintz, H. Zhao, M. J. Bazile, and K. R. Dunbar, Chem. Mater. **15**, 1840 (2003).

[14] L. R. Melby, R. J. Harder, W. R. Hertler, W. Mahler, R. E. Benson, and W. E. Mochel, J. Am. Chem. Soc. **84**, 3374 (1962).

[15] H. Zhao, R. A. Heintz, X. Ouyang, K. R. Dunbar, C. F. Campana, and R. D. Rogers, Chem. Mater. **11**, 736 (1999).

[16] H. Zhao, R. A. Heintz, K. R. Dunbar, and R. D. Rogers, J. Am. Chem. Soc. **118**, 12844 (1996).

[17] J. S. Miller, J. C. Calbrese, R. S. Mclean, and A. J. Epstein, Adv. Mater. **4**, 498 (1992).

[18] W. Hibbs, D. K. Rittenburg, K.-I. Sugiura, B. M. Burkhart, B. G. Morin, A. M. Arif, L. Liable-Sands, A. L. Rheingold, M. Sundaralingam, A. J. Epstein, and J. S. Miller, Inorg. Chem. **40**, 1915 (2001).

[19] S. J. Etzkorn, W. Hibbs, J. S. Miller, and A. J. Epstein, Phys. Rev. Lett. **89**, 207201 (2002).

[20] S. J. Etzkorn, W. Hibbs, J. S. Miller, and A. J. Epstein, Polyhedron. **22**, 1751 (2003).

[21] S. J. Etzkorn, W. Hibbs, J. S. Miller, and A. J. Epstein, Phys. Rev. B **70**, 134419 (2004).

[22] R. C. Thompson, Y. Hoyano, and C. F. Schwerdtfeger, Solid State Commun. **23**, 633 (1977).

[23] R. C. Thompson, V. K. Gujral, H. J. Wagner, and C. F. Schwerdtfeger, Phys. Status Solidi A **53**, 181 (1979).

[24] E. B. Vickers, I. D. Giles, and J. S. Miller, Chem. Mater. **17**, 1667 (2005).

[25] J. M. Manriquez, J. S. Miller, and A. Epstein, Science **252**, 1415 (1991).

[26] K. I. Pokhodnya, D. Pejakovic, A. J. Epstein, and J. S. Miller, Phys. Rev. B **63**, 174408 (2001).

[27] P. Zhou, B. G. Morin, J. S. Miller, and A. J. Epstein, Phys. Rev. B **48**, 1325 (1993).

[28] B. G. Morin, P. Zhou, C. Hahm, A. J. Epstein, and J. S. Miller, J. Appl. Phys. **73**, 5648 (1993).

[29] M. D. Harvey, T. D. Crawford, and G. T. Yee, Inorg. Chem. **47**, 5649 (2008).

[30] D. Dolphin, W. Pegg, and P. Wirz, Can. J. Chem. **52**, 4078 (1974).

[31] See Supplemental Material at http://link.aps.org/supplemental/10.1103/PhysRevB.92.184431 for more data/analysis on the PXRD, SEM, magnetization and heat capacity measurements.

[32] J. Rodriguez-Carvajal, Physica B **192**, 55 (1993).

[33] P.-E. Werner, L. Eriksson, and M. Westdahl, J. Appl. Cryst. **18**, 367 (1985).

[34] A. L. Patterson, Phys. Rev **56**, 978 (1939).

[35] A. Furrer, J. Mesot, and T. Strässle, *Neutron Scattering in Condensed Matter Physics*, Series on Neutron Scattering Techniques and Applications, Vol. 4 (World Scientific, Singapore, 2009).

[36] T. C. Tseng, N. Abdurakhmanova, S. Stepanow, and Klaus Kern, J. Phys. Chem. C **115**, 10211 (2011).

[37] A. Berlie, Ph.D. thesis, Durham University, UK, 2013.

[38] C. Kittel, *Introduction to Solid State Physics*, 8th ed. (John Wiley and Sons, Inc, Hoboken, NJ, 2005).

[39] S. Ohkoshi, T. Iyoda, A. Fujishima, and K. Hashimoto, Phys. Rev. B **56**, 11642 (1997).

[40] K. Mandal, S. Mitra, and P. Anil Kumar, Europhys. Lett. **75**, 618 (2006).

[41] C. Peng, S. Zhang, G. Li, and D. Dai, J. Appl. Phys. **76**, 998 (1994).

[42] J. S. Kouvel and H. Brooks, Office of Naval Research, Technical Report No. 198, Harvard University, 1954.

[43] M. Perovic, A. Mrakovic, V. Kusigerski, J. Blanusa, and V. Spasojevic, J. Nanopart. Res. **13**, 6805 (2011).

[44] D. Hüser, L. E. Wenger, A. J. van Duyneveldt, and J. A. Mydosh, Phys. Rev. B **27**, 3100 (1983).

[45] D. Peddis, D. Rinaldi, G. Ennas, A. Scano, E. Agostinelli, and D. Fiorani, Phys. Chem. Chem. Phys. **14**, 3162 (2012).

[46] P. C. Fannin, B. K. P. Scaife, and S. W. Charles, J. Phys. D: Appl. Phys. **21**, 533 (1988).

[47] P. C. Fannin, L. Choen-Tannoudji, E. Bertrand, A. T. Giannitsis, C. Mac Oireachtaigh, and J. Bibette, J. Magn. Magn. Mater. **303**, 147 (2006).

[48] F. Ludwig, A. Guillaume, M. Schilling, N. Frickel, and A. M. Schmidt, J. Appl. Phys. **108**, 033918 (2010).

[49] P. M. Lahti, *Magnetic Properties of Organic Materials* (Marcel Dekker, New York, 1999).

[50] M. Sorai, Y. Nakazawa, M. Nakano, and Y. Miyazaki, Chem. Rev. **113**, PR41 (2013).

[51] M. Nakano and M. Sorai, Chem. Phys. Lett. **169**, 27 (1990).

[52] L. Wang, K. Vu, A. Navrotsky, R. Stevens, B. F. Woodfield, and J. Boerio-Goates, Chem. Mater. **16**, 5394 (2004).

[53] H. Lei, J. Li, and J. Luo, Nanoscale **7**, 6762 (2015).

[54] *Muon Science: Muons in Physics, Chemistry and Materials*, edited by S. L. Lee, S. H. Kilcoyne, and R. Cywinski (Institute of Physics Publishing, London, 1998).

[55] F. L. Pratt, S. J. Blundell, Th. Jestädt, B. W. Lovett, R. M. Macrae, and W. Hayes, Magn. Reson. Chem. **38**, S27 (2000).

[56] A. Berlie, I. Terry, S. Giblin, T. Lancaster, and M. Szablewski, J. Appl. Phys. **113**, 17E304 (2013).

[57] B. W. Lovett, S. J. Blundell, F. L. Pratt, Th. Jestädt, W. Hayes, S. Tagaki, and M. Kurmoo, Phys. Rev. B **61**, 12241 (2000).

[58] M. Imada, A. Fujimori, and Y. Tokura, Rev. Mod. Phys. **70**, 1039 (1998).

[59] J. Wu and C. Leighton, Phys. Rev. B **67**, 174408 (2003).

[60] M. Ulrich, J. Garcia-Otero, J. Rivas, and A. Bunde, Phys. Rev. B **67**, 024416 (2003).

[61] I. A. Campbell, A. Amato, F. N. Gygax, D. Herlach, A. Schenk, R. Cywinski, and S. H. Kilcoyne, Phys. Rev. Lett. **72**, 1291 (1994).

[62] J. Park, E. Lee, N. Hwang, M. Kang, S. C. Kim, Y. Hwang, J. Park, H. Noh, J. Kim, J. Park, and T. Hyeon, Angew. Chem., Int. Ed. **44**, 2872 (2005).

[63] M. Evangelisti, T. G. Sorop, O. N. Bakharev, D. Visser, A. D. Hillier, J. J. Alonso, M. Haase, L. A. Boatner, and L. Jos de Jongh, Phys. Rev. B **84**, 094408 (2011).

[64] J. Gutiérrez, F. J. Bermejo, J. M. Barandiarán, S. P. Cottrell, P. Romano, C. Mondelli, J. R. Stewart, L. Fernández Barquín, and A. Peña, Phys. Rev. B **73**, 054433 (2006).

[65] T. Lancaster, S. J. Blundell, P. J. Baker, H. J. Lewtas, W. Hayes, F. L. Pratt, H. T. Yi, and S. W. Cheong, Phys. Rev. B **80**, 020409 (2009).